Incorporation of modified Stöber silica nanoparticles in polystyrene/polyamide-6 blends: Coalescence inhibition and modification of the thermal degradation via controlled dispersion at the interface

T. Parpaite, B. Otazaghine, A. Taguet, Rodolphe Sonnier, A. S. Caro-Bretelle, José-Marie Lopez-Cuesta

Incorporation of modified Stöber silica nanoparticles in polystyrene/polyamide-6 blends: Coalescence inhibition and modification of the thermal degradation via controlled dispersion at the interface

T. Parpaite, B. Otazaghine*, A. Taguet, R. Sonnier, A.S. Caro, J.M. Lopez-Cuesta

Centre des Matériaux des mines d'Alès, 6, avenue de Clavières, 30319 Alès, France

A B S T R A C T

The controlled dispersion of Stöber silica nanoparticles (SiNPs) at the interface of a PS/PA6 (80/20 wt%) blend was achieved by means of surface modifications using 3-methacryloxypropyltrimethoxysilane (MPS). The final localization of SiNPs in the blend was predicted using wetting parameter calculation and confirmed by scanning electronic microscopy (SEM) observations. Stability of blends during annealing was evaluated qualitatively by laser diffraction particle size analyzer. Morphologies of the blends in the molten state were observed using optical microscopy. Flammability of blends was investigated using pyrolysis-combustion flow calorimeter (PCFC). Results showed that both microstructure stability during annealing and thermal degradation of the blend, were improved when MPS-modified SiNPs are located at the interface. SEM pictures revealed that the MPS-modified SiNPs form a solid barrier between PS and PA6 phases which inhibits coalescence process and modifies the thermal degradation mechanisms.

Keywords:
Silica nanoparticles
Selective dispersion
Compatibilization

1. Introduction

The improvement of polymer properties by blending is a widely used and well-known technique. However immiscibility of polymers is a recurring issue of most polymer blends due to the high interfacial tension of these systems. To decrease interfacial tensions, a wide range of interfacial agents [1,2] such as block [3] or grafted [4] copolymers or reactive compatibilizers [5,6] could be used. Properties of the resulting compatibilized blends depend on the molecular architecture of the organic compatibilizers [7,8]. For example, residual presence of low molecular weight stabilizers in the matrix due to micellization [9,10] or interface desorption during high shear process [11,12] degrades mechanical properties [13,14]. To overcome these drawbacks, intense research efforts to find novel and better kinds of compatibilizers are still investigated. One of the possible alternative routes is to selectively disperse solid nanoparticles (NPs) at the interface to stabilize the blend. Indeed, Lipatov and Nesterov [15] showed that solid fillers can play the role of stabilizer for immiscible polymer mixtures. Since this pioneering work, the number of studies dealing with compatibilizing effect of solid fillers in polymer blends has increased dramatically. However, the understanding of the different mechanisms of stabilization is still an intensive topic of research.

Recently, Fenouillot et al. [16] published an interesting review discussing similarities and differences between mechanisms involved in the stabilization of low and high viscous polymer emulsions containing solid particles. For low viscosity emulsion systems the "Pickering effect" [17] is commonly recognized as the main mechanism to explain the stabilization. This effect corresponds to the inhibition of the coalescence between dispersed liquid drops due to the presence of a mechanical barrier of solid particles at the interface. In these liquid emulsions, the thermodynamic equilibrium is easily reached and drives the localization of fillers in the blend. However final localization of solid fillers into viscous polymers blend is a complex balance between thermodynamic driving forces and kinetic considerations. From a thermodynamic point of view, the localization of the NPs in such ternary system depends on the values of surface tension of blend components (i.e. two polymers and one solid filler) [16,18]. But, due to the high viscosity of a molten polymer matrix, thermodynamic equilibrium may be reached only for long times. Hence, kinetic factors must be considered. They can be due to (i) the process, such as the mixing sequences [19–22], the shear forces [21,23] and time of mixing [24,25], to (ii) the specific parameters of the polymers blend

* Corresponding author.
E-mail address: belkacem.otazaghine@mines-ales.fr (B. Otazaghine).

such as the viscosity ratio [25–27], or to (iii) the specific parameters of the fillers such as the size [16,28–30], the shape [31,32], and the surface chemistry [33–36]. The effect of viscosity ratio governs the particle distribution when the interfacial tension between the two polymers is not too high. Otherwise, the thermodynamic interactions are predominant [37].

When localized at the interface between two immiscible polymers, fillers can play the role of compatibilizer. Organoclays [38–43] and fumed silica [44–47] are the most commonly used nanoparticles to compatibilize polymer blends. Most frequently, presence of solid fillers at the interface of a blend induces a reduction of the size distribution of the dispersed phase [48–50]. The ability of silica nanoparticles (SiNPs) to significantly decrease the apparent interfacial tension has been clearly reported [19] whereas the high aspect ratio of organoclays is more favorable to inhibit coalescence by creating a physical barrier against coalescence [39,42,48]. Indeed, as platelets exhibit a higher aspect ratio, they are most likely to cover the interface between two immiscible polymers than spherical shape fillers. It must be noted that in the case of a blend where solid particles are not only distributed at the interface, i.e. some NPs are present in the dispersed phases and/or in the matrix, the morphology refinement observed can also be due to the modification of the viscosity ratio between both polymers.

As mentioned previously, the surface chemistry of NPs has a dramatic influence on their localization in the blend and hence on the compatibilizing role and on the final properties. In most cases, the localization of NPs at the interface is not really accurate and the size and surface chemistry are not well-controlled parameters. This is only in the past few years, that authors started to develop new NPs with desired surface properties in order to control their localization and dispersion in polymer blends [33–36]. Very recently, Huang et al. [51] clearly identified that silica nanoparticles (SiNPs) grafted with low molecular weight PS macromolecules migrated at the interface of a PMMA/SAN blend, whereas SiNPs modified with high molecular weight PS chains migrated to the PMMA phase due to a lower interfacial tension. In the same manner, Chung et al. [33] incorporated SiNPs modified with PMMA chains in poly(methylmethacrylate)/poly(styrene-*ran*-acrylonitrile) 50/50 blends. They demonstrated that, when the PMMA brush length increased the SiNPs migrated from the interface to the PMMA phase. Contact angles measurements showed that SiNPs became more hydrophilic as the grafted PMMA brush length increased. All these relatively recent articles do not mention any measurement of the final performances of the synthesized material such as thermal, mechanical or fire properties.

The main objective of the present work is to highlight the effect of the selective dispersion of mesoporous SiNPs on final properties of immiscible PS/PA6 blend. Therefore, the use of tailored homemade SiNPs was motivated in order to have a full control on the properties of the incorporated SiNPs from synthesis to surface modifications. Their final localization at the interface was achieved with the help of thermodynamic predictions and was clearly confirmed by SEM observations. Finally, mechanisms involved in the improvement of thermal stability of microstructure and thermal degradation behavior are discussed.

2. Materials and methods

2.1. Materials

CRISTAL 1340 polystyrene (PS) was purchased from Total Petrochemicals (Feluy, Belgium). It is a crystal PS with a high molecular weight and a melt flow index (MFI) of 4 g 10 min^{-1} (with 5 kg at 200 °C). Ultramid B3K polyamide-6 (PA6) was supplied by BASF (Wyandotte, USA). Its melting point temperature is 220 °C (ISO Test Method 3146) and its MFI is 160 g 10 min^{-1} (with 5 kg at 275 °C). Polymer pellets were dried under vacuum at 80 °C for 12 h before processing.

Tetraethoxysilane (TEOS, 99.9%), ethanol (EtOH, 96%), ammonia (NH_3, 28%) and 3-methacryloxypropyltrimethoxysilane (MPS, 99.9%) were used as purchased from Rectapur, Sigma–Aldrich, Merck and, Wackers Silicon, respectively.

2.2. Synthesis of monodisperse silica nanoparticles via Stöber method

Silica nanoparticles (SiNPs) were prepared using a modified Stöber method [52]. Into a 100 ml glass reactor were introduced 41.09 g of ethanol solution 96% ([EtOH] = 1.1 M), 1.77 g of aqueous ammonia solution 28% wt ([NH_3] = 0.8 M) and 0.05 g of water ($[H_2O]_{total}$ = 3.3 M). The reactor was then placed under magnetic stirring of 500 rpm and heated at 55 °C. After 10 min, 1.65 g of TEOS ([TEOS] = 0.17 M) as silica precursor was quickly added to the mixture. Reaction took place in 2 h keeping the same conditions (55 °C, 500 rpm) to complete the hydrolysis-condensation of all TEOS molecules into mesoporous SiNPs. Ethanol was removed and replaced by water using successive evaporations of ethanol under vacuum. Finally the aqueous solution was lyophilized and the obtained particles were called bare silica nanoparticles (bare-SiNPs).

2.3. Surface modification of silica nanoparticles

At the end of synthesis of SiNPs by Stöber method (before purification), the obtained suspension was treated using MPS silane coupling agent. The mixture was cooled at room temperature and the silane coupling agent (10% of the total weight of SiNPs) and water (the ethanol/water ratio was modified to 9/1) were added. The solution was kept under magnetic stirring (500 rpm) 1 h at room temperature and then heated at ethanol reflux overnight. Finally, ethanol was removed and replaced by water using successive evaporations of ethanol under vacuum. The aqueous solution was lyophilized and the modified particles obtained were called grafted silica nanoparticles (grafted-SiNPs).

2.4. Nanocomposite compounding procedure

Bare and grafted SiNPs were incorporated into a PS/PA6 immiscible polymer blend by using a DSM twin-screw mini-extruder. The total mass of polymer used for each blend was 12 g. The weight ratio between PS and PA6 was 80/20 (wt%) and SiNPs content was fixed at 3 wt%. In the following, the PS/PA6 80/20 blend without SiNPs is noted unfilled blend, whereas PS/PA6 blends filled with 3 wt% of bare and grafted SiNPs are noted bare-SiNPs blend and grafted-SiNPs blend, respectively.

To avoid handling of dry nanoparticles powders, we used in a first step a solvent casting method to embed SiNPs into PS film. A small fraction of PS matrix (1 g) was dissolved in 10 ml of THF and mixed with SiNPs at room temperature during 12 h under magnetic stirring. The solvent was then evaporated and the obtained film was dried under vacuum at 80 °C for 24 h (Supporting information).

The second step was the extrusion of the nanocomposites. Concerning the order of mixing steps, the PS film containing the SiNPs was first pre-compounded with the rest of PS pellets for 1 min, and then PA6 dispersed phase was added and mixed for 4 min. Screw speed and temperature were kept constant at 40 rpm and 250 °C, respectively. At the beginning of the mixing process the SiNPs are present only into the PS matrix, so the migration process of the SiNPs can be easily highlighted. The screw speed was also varied from 40 to 120 rpm for the preparation of the unfilled blend

in order to evidence the influence of the shear forces during extrusion on the morphology of the system.

2.5. Annealing and selective extraction

After extrusion, annealing was performed using TGA. Around 20 mg of blend was annealed at process temperature (250 °C) for 10 min under nitrogen flow. Then the annealed materials were immersed into 10 ml of THF at room temperature without stirring overnight to remove PS. Finally, PA6 nodules were purified by three washing/centrifugation cycles using THF solvent and then collected for analysis.

2.6. Characterizations

2.6.1. Thermogravimetric analysis (TGA)

The thermal decomposition curves of polymers and SiNPs were obtained using a Perkin Elmer Pyris-1 instrument. Weight loss (%) and mass loss rate (MLR) of sample were plotted as a function of degradation temperature. For SiNPs, an isothermal step (1 h, 100 °C) was carried out before starting the analysis in order to remove physisorbed water then, measurements were performed under air flow with a heating rate of 10 °C min^{-1}. For polymer materials both, air and nitrogen atmospheres were used with a heating rate of 60 °C min^{-1} in order to be comparable to PCFC test conditions. All measurements were performed in the range 100–700 °C. Total mass loss of sample at 700 °C and peak of MLR were recorded and noted TML and pMLR, respectively. The sample weight was 10 ± 1 mg.

2.6.2. Scanning electron microscopy

A Scanning Electron Microscopy (FEI Quanta 200 ESEM) was used to observe SiNPs with or without surface modification and to evaluate the final localization of these fillers in the blends. All micrographs were recorded under high vacuum. SiNPs were directly observed from diluted latex at the end of synthesis (Supporting information) or at the dry state (powders) after purification. Polymer blend samples were prepared using cryo-fractured or polished cross-section.

2.6.3. Dynamic light scattering (DLS)

A Malvern Nano ZS DLS apparatus was used to determine hydrodynamic diameter (Z-average) and polydispersity index (PDI) of SiNPs. Water was used as dispersant, temperature of measurement was 25 °C, and equilibration time was 120 s. Common values of refractive and absorption indices for silica (1.45 and 0.01, respectively) were used. At least, three measurements were performed for each sample to ensure repeatability.

2.6.4. Laser diffraction particle size analyzer

A Coulter LS 13230 (Coulter Beckmann Co.) laser diffraction particle size analyzer instrument was used to determine the size distribution of extracted PA6 nodules. The PA6 nodules were collected after dissolving the PS matrix using THF solvent. Size measurements were performed using the micro liquid module (MLM, 15 ml) in THF, obscuration was 10 ± 2%. At least, three measurements were performed for each sample. Laser diffraction particle size analyzer is an interesting alternative method to characterize dispersed phases in immiscible polymer blends. In fact, the number of dispersed phases analyzed is much larger than with conventional images analysis from electron microscopy observations (SEM or TEM).

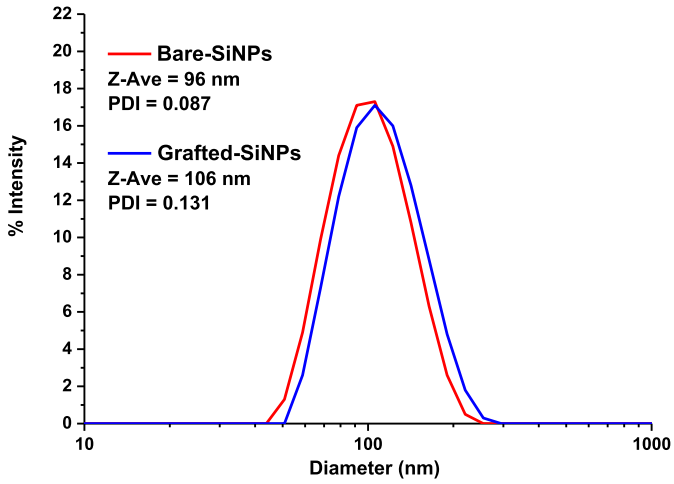

Fig. 1. Size distribution by DLS of bare and grafted SiNPs.

2.6.5. Optical microscopy observations in the molten state

Morphologies of blends in the molten state were observed by optical microscopy with a Laborlux 11 pol S apparatus (Leitz) equipped with a Mettler FP82HT hot stage. Thin cut sections of blends were melted at 250 °C during 10 min and then investigated in transmission mode at room temperature. Images were recorded using a 3-CDD camera (768 × 576 pixels) JVC KY-F55B.

2.6.6. Contact angle measurement

Contact angle measurements were carried out by depositing a liquid drop with controlled volume on the sample surface. The contact angle θ between the liquid and the substrate was measured using a Digidrop GBX goniometer apparatus equipped with a CDD camera. Thin flat disks of 25 mm of pure polymers and SiNPs were prepared using a compression molded laboratory press at 250 °C for 3 min with a constant pressure of 10 bars [53]. Then, contact angle measurements between sample flat surface (polymers or compacted SiNPs) and three solvents (water, formamide and diiodomethane) with different dispersive (γ_L^d) and polar (γ_L^p) contributions were performed three times for each surface–solvent pair. The dispersive (γ_S^d) and polar (γ_S^p) contributions to the surface energy of sample were calculated according to Equation (1) using the Owens–Wendt approach [54].

$$\gamma_L = (1 + \cos\theta) = 2\sqrt{\gamma_S^d \gamma_L^d} + 2\sqrt{\gamma_S^p \gamma_L^p} \quad (1)$$

where γ_L^d and γ_L^p are known for the three different liquids used.

2.6.7. Pyrolysis combustion flow calorimeter (PCFC)

Flammability of samples was investigated using a pyrolysis-combustion flow calorimeter (Fire Testing Technology). This technique was developed by Lyon and Walters [55] in order to study the thermal degradation of samples at the microscale. Sample weights are around 2 ± 0.5 mg. Samples are first pyrolyzed at 1 °C s^{-1} and the degradation products are sent into a combustor at 900 °C where the products are completely oxidized. The estimation of rate of heat release is performed by means of oxygen consumption measurements according to Huggett's relation [56]. In the case of oxidative pyrolysis, inert gas flow in pyrolysis chamber is replaced by air flow. Typical PCFC analysis plots the heat release rate (HRR) as a function of pyrolysis temperature. The values of peak of Heat Release Rate (pHRR), temperature at pHRR (T_{peak}), Total Heat Released (THR) which is the integral of the heat release rate over the duration of the experiment, were also measured. Using peak of mass loss rate

(pMLR) and total mass loss (TML) measured by TGA the instantaneous effective heat of combustion (noted EHC_i) can be calculated and the mean effective heat of combustion (noted EHC_m) according the following Equations (2) and (3):

$$pHRR = pMLR \times EHC_i \quad (2)$$

$$THR = TML \times EHC_m \quad (3)$$

3. Results and discussion

3.1. Silica nanoparticles: size distribution and amount of grafting

At the end of the Stöber procedure, milky latex was obtained. Size distributions of bare-SiNPs and grafted-SiNPs are plotted in Fig. 1. The hydrodynamic radius (Z-Ave) of the SiNPs increases from 96 to 106 nm after grafting process due to the presence of MPS molecules onto the surface (Fig. 2). This slight increase of the measured DLS diameter is characteristic of the presence of polymer coating onto the SiNPs [57]. Values of polydispersity index of bare-SiNPs and grafted-SiNPs equal to 0.087 and 0.131, respectively (Fig. 1) reveal the monodispersity of produced samples.

TGA measurements were performed to estimate the quantity of silane coupling agent covalently anchored onto the surface of grafted-SiNPs. Fig. 3 displays the weight loss (%) and the associated derivate weight (%/min) for bare and grafted SiNPs as a function of temperature. The residue at 700 °C of bare-SiNPs is 93.3%. This weight loss corresponds to the slow condensation of silanol groups (Si—OH). According to the literature, this mass loss could be decomposed in two steps [58,59]. The mass loss observed in the temperature range 200—400 °C is assigned to the condensation of surface hydroxyl groups whereas isolated hydroxyl groups (inside the mesoporous structure) are decomposed at higher temperatures (up to 450 °C). In the case of grafted-SiNPs, residue at 700 °C is 88.7%. This additional weight loss of 4.9% for grafted-SiNPs compared to the bare ones is related to the presence of MPS. The thermal degradation behavior of MPS was also studied in the literature [60,61]. First, cleavage of C—O bonds occurs in the temperature range 150—400 °C (methacrylate acid mass loss) followed by the cleavage of Si—C bonds (allylic radical mass loss). Finally, up to 500 °C, complete oxidation of silane groups of MPS molecules and condensation of isolated hydroxyl groups of SiNPs happen simultaneously. This amount of organic compound corresponds to a multilayer grafting (see Fig. 2) because of the hydroxylation and condensation of MPS molecules in the presence of water during grafting process [62].

The presence of an organic layer around grafted-SiNPs is also confirmed by SEM analysis of SiNPs powders (Fig. 4). In fact, monodisperse spherical SiNPs are known to be able to form well-ordered arrangement upon solvent evaporation [63]. However, the formation of this kind of ordered three-dimensional network strongly depends on electrostatic and capillary interactions [64]. So, the well-ordered assembly observed in Fig. 4a is due to the Van der Waals (VDW) interactions between surface silanol groups but also confirms the good monodispersity of the bare-SiNPs produced. On the contrary, the presence of MPS molecules onto the surface of grafted-SiNPs inhibits the VDW interactions and generates steric repulsion effects between terminal methacrylate groups of MPS molecules. As a consequence, grafted-SiNPs appear less organized compared to the bare ones. This disruption of organization proves also the surface modification of the SiNPs.

3.2. Wetting parameter calculations

According to thermodynamics, the localization of solid fillers into an immiscible polymer blend is governed by the surface tensions of the different components of the blend. Considering a spherical solid particle (S) at the interface of two immiscible media (Fig. 5), *A* and *B* (liquid or polymer) it is possible to define a wetting parameter, ω, from the contact angle θ as a function of interfacial tensions of blend (Equation (4)) [16]. This model is based on the hypothesis that free interfacial energy of the system ΔG is equal to 0 at thermodynamic equilibrium.

$$\omega_{AB} = \cos\theta = \frac{\gamma_{SB} - \gamma_{SA}}{\gamma_{AB}} \quad (4)$$

where γ_{ij} is the interfacial tension between components *i* and *j*, *A* and *B* are polymer materials, and S a solid filler.

Also, the wetting parameter of a solid particle S into a binary immiscible polymer blend (*A* and *B*) expresses the most favorable position of the solid filler in order to minimize the free interfacial energy of the blend. Consequently, according to the value of ω it is possible to predict the final localization of S. If $\omega_{AB} > 1$, solid fillers are dispersed only in polymer *A*. On the contrary, if $\omega_{AB} < -1$, solid fillers are dispersed only in polymer *B*. Finally, when $-1 < \omega_{AB} < 1$ solid fillers are supposed to be segregated at the interface.

However, if there are several experimental techniques to evaluate polymer/polymer interfacial tensions [65], determination of filler/polymer interfacial tensions remains a challenge especially in the case of nanofillers. Hence, theoretical models like Owens—Wendt model [54] (Equation (5)) are usually used for calculating interfacial tensions.

$$\gamma_{ij} = \gamma_i + \gamma_j - 2\sqrt{\gamma_i^d \gamma_j^d} - 2\sqrt{\gamma_i^p \gamma_j^p} \quad (5)$$

where γ_i^d and γ_i^p are dispersive and polar contributions to the total surface tension γ_i, respectively.

The values of surface tension used for wetting parameter calculations are listed in Table 1. Because of the high polarity of bare-SiNPs it was not possible to properly measure contact angle of this sample due to strong adsorption of water during experiment. Consequently, we used values from the literature [26]. Interestingly

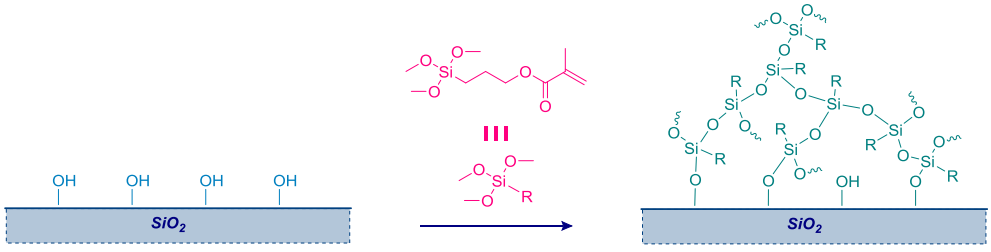

Fig. 2. Schematic representation of the multilayer grafting process of MPS molecules onto silica surface in the presence of water.

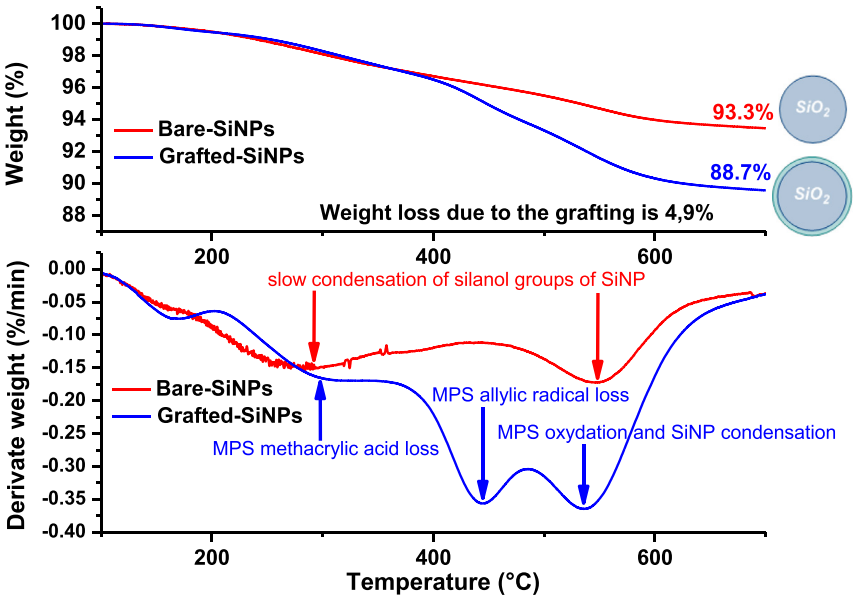

Fig. 3. TGA curves of bare (in red) and grafted (in blue) SiNPs. (For interpretation of the references to color in this figure legend, the reader is referred to the web version of this article.)

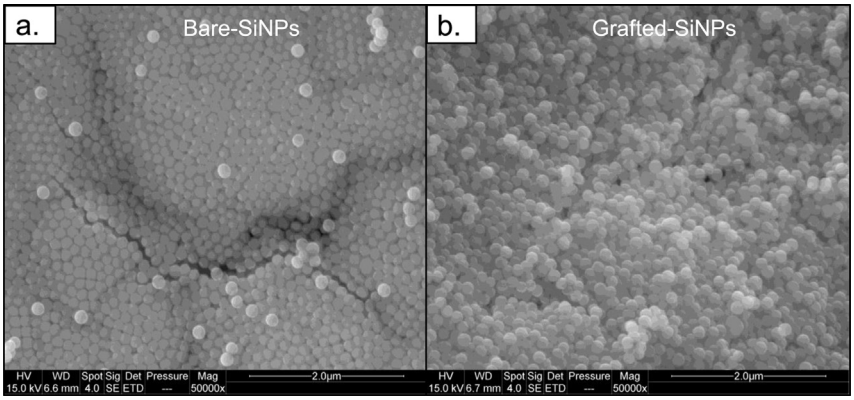

Fig. 4. Topographic micrographs of bare (a) and grafted (b) SiNPs powders.

enough, the surface tension value measured for MPS grafted silica is very close to the one found in the literature for MPS modified cellulosic fiber with similar contact angle method [66] and noted MPS grafted cellulose fibers in Table 1.

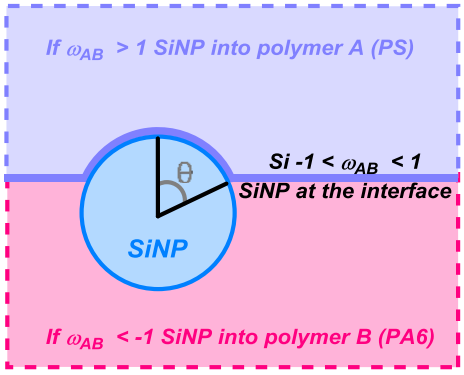

Fig. 5. Wetting parameter of solid filler at the interface of immiscible polymers.

According to wetting parameter calculations reported in Table 1, bare-SiNPs are supposed to be dispersed only in the PA6 phase ($\omega_{AB} = -1.96$) whereas the grafted ones should be segregated at the interface ($\omega_{AB} = 0.10$). It is necessary to notice that these thermodynamic predictions are only true if the system equilibrium can be reached without kinetic disturbance related to mixing procedure or viscosity ratio between polymers [26].

3.3. Final localization of nanoparticles

Morphology of the unfilled PS/PA6 blend was observed by SEM. PA6 nodules are well-dispersed in the PS matrix (Fig. 6).

In order to highlight migration process during mixing, SiNPs were pre-compounded with the PS matrix. So we can assume that all nanofillers are initially dispersed in the PS matrix.

SEM micrographs in Fig. 7 clearly show that the final localization of SiNPs depends on their surface chemistry. In fact, bare-SiNPs (left column) have totally migrated from the PS matrix to the dispersed PA6 nodules whereas grafted-SiNPs (right column) are located at the interface. These microscopic observations are in good agreement with the previous thermodynamic predictions obtained using

Table 1
Surface tension values of components of the blends.

Material	γ_i (mN/m)	γ_i^d (mN/m)	γ_i^p (mN/m)	ω_{AB}
PS	31.9	11.3	20.7	–
PA6	41.2	8.8	32.4	–
Bare-SiNPs[a]	80.0	29.4	50.6	−1.96
Grafted-SiNPs	67.1	31.7	35.5	0.10
MPS grafted cellulose fiber[b]	69	32	37	–

[a] From Ref. [26].
[b] From Ref. [66].

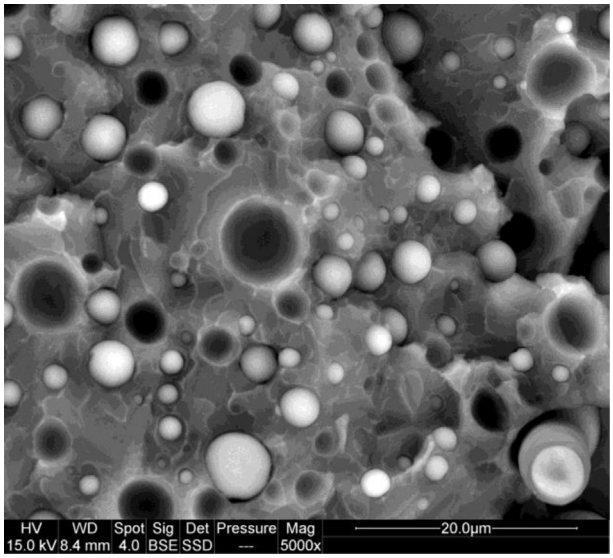

Fig. 6. Micrograph of fractured surface of neat PS/PA6 80/20 blend, PA6 nodules (in white) are well-dispersed in the PS matrix (in gray).

wetting parameter. Moreover, in the case of the blend filled with bare-SiNPs, voids (white ellipse on Fig. 7a–c) are formed, revealing a poor interfacial adhesion between the two polymers. On the contrary, when grafted-SiNPs are located at the interface (white arrows on Fig. 7b–d) no decohesion is observed. The same tendency is noticed on cryo-fractured surfaces micrographs (Fig. 7e,f). In fact, PA6 nodules covered by grafted-SiNPs seem embedded in the PS matrix (Fig. 7b), whereas in the case of PA6 nodules containing bare-SiNPs decohesion appears, numerous nodules have been ejected during sample preparation (black holes indicated by black arrows on Fig. 7e). Note that poor interfacial adhesion is also observed for the unfilled blend (Fig. 6).

3.4. Morphology of the PA6 dispersed phase

Most frequently, the size distribution of the dispersed phase in polymer blends is evaluated using microscopic analysis and image analysis at the center of the extrudate in the perpendicular direction to polymer flow. In these conditions only spherical nodules are observed (Fig. 8a). In fact, due to the fountain-flow process (Fig. 8c), at the center of the polymer flow, shear rate is very low and consequently dispersed phases are spherical. On the other hand, shear rates are maximum in the skin region of the extrudate between the frozen layer and the core polymer flow. These important shear rates produce elongated nodules parallel to the extrusion direction (white arrows in Fig. 8b,c).

To characterize these two populations of nodules (spherical and elongated), laser diffraction particle size analyzer was used as an alternative technique to classical image analysis [8]. The PA6 nodules were collected after dissolving the PS matrix using THF solvent and their size distribution was measured. Fig. 9 highlights the sensitivity of the method to the aspect ratio of PA6 nodules. Because the algorithm of calculation is based on the hypothesis of perfect spheres (Mie theory), a well-defined Gaussian distribution indicates the presence of monodisperse particles with a low aspect ratio. On the contrary, a broad size distribution of spherical particles and/or presence of elongated particles can be noticed in the 10–100 μm range. Typical "M" shape curves for particles with a very high aspect ratio can be obtained, lower and higher peaks corresponding to the lower and higher diameters of particles with high aspect ratio, respectively. Moreover, the aspect ratio of elongated particles generated during extrusion in the skin polymer layer (Fig. 8c) is shear rate dependent. That's why the elongated PA6 nodules are mainly obtained for the higher screw speed also corresponding to the higher shear rate during extrusion process.

To conclude, two populations of nodules should be considered: spherical PA6 nodules in the range 0–10 μm and elongated ones in the range 10–100 μm. These statements are in concordance with micrographs of cross polished section parallel to the extrusion direction (Fig. 8b) and the corresponding extracted PA6 nodules (Fig. 10a).

3.5. Thermal stability of microstructure

Usually, in the case of uncompatibilized polymer blends, a quiescent annealing of 10 min around the temperature of process is enough to observe a significant coalescence phenomenon [67]. Hence, the blends are thermally annealed in TGA oven for 10 min at 250 °C under nitrogen flow. Comparison of the size distribution of dispersed PA6 nodules before and after annealing is an interesting qualitative way to monitor the evolution of the microstructure. Left column of Fig. 11 displays the size distributions of PA6 nodules before (filled curves) and after (dotted curves) annealing for each blends. As explained previously, two populations of nodules are present in the extrudate. Consequently, two phenomena could occur during annealing. First one is the coalescence process which mainly concerns the small spherical nodules, second one is the relaxation process of elongated nodules (filled white arrows in Fig. 10a) in large spherical ones (dotted white arrows in Fig. 10b) [45]. Both phenomena tend to decrease the free interfacial energy of the system. For example, in the case of the unfilled blend both relaxation and coalescence processes are observed (upper left in Fig. 11). In fact, a decrease of the volume fraction of the small spherical nodules (1–6 μm) is recorded. In the same time, an increase of the volume fraction of biggest PA6 nodules (6–20 μm) is observed. This decrease of the volume fraction of small PA6 nodules combined with the apparition of bigger ones (vertical dashed arrows in Fig. 11) is characteristic of the coalescence process. The relaxation of the elongated nodules is observed from the shift and refinement of the broad peak (20–50 μm) which is indicated by horizontal filled arrow on the graphs of Fig. 11.
When SiNPs are added to the system, both the initial size distribution and the evolution of the morphology during annealing are affected. For the bare-SiNPs blend (middle row), the break-up/coalescence mechanism is probably modified due to the total migration of bare-SiNPs inside PA6 nodules which increases the viscosity of the dispersed phase. Hence, the PA6 nodules are more difficult to stretch. Consequently, no more elongated nodules are observed. During annealing the coalescence process seems stronger in the 20–30 μm range. Finally, in the case of grafted-SiNPs blend (lower row) the volume fraction of small spherical nodules (<10 μm) before and after annealing is unchanged. This means that coalescence is prevented. The stabilization of the microstructure against annealing is attributed to the formation of a solid barrier of

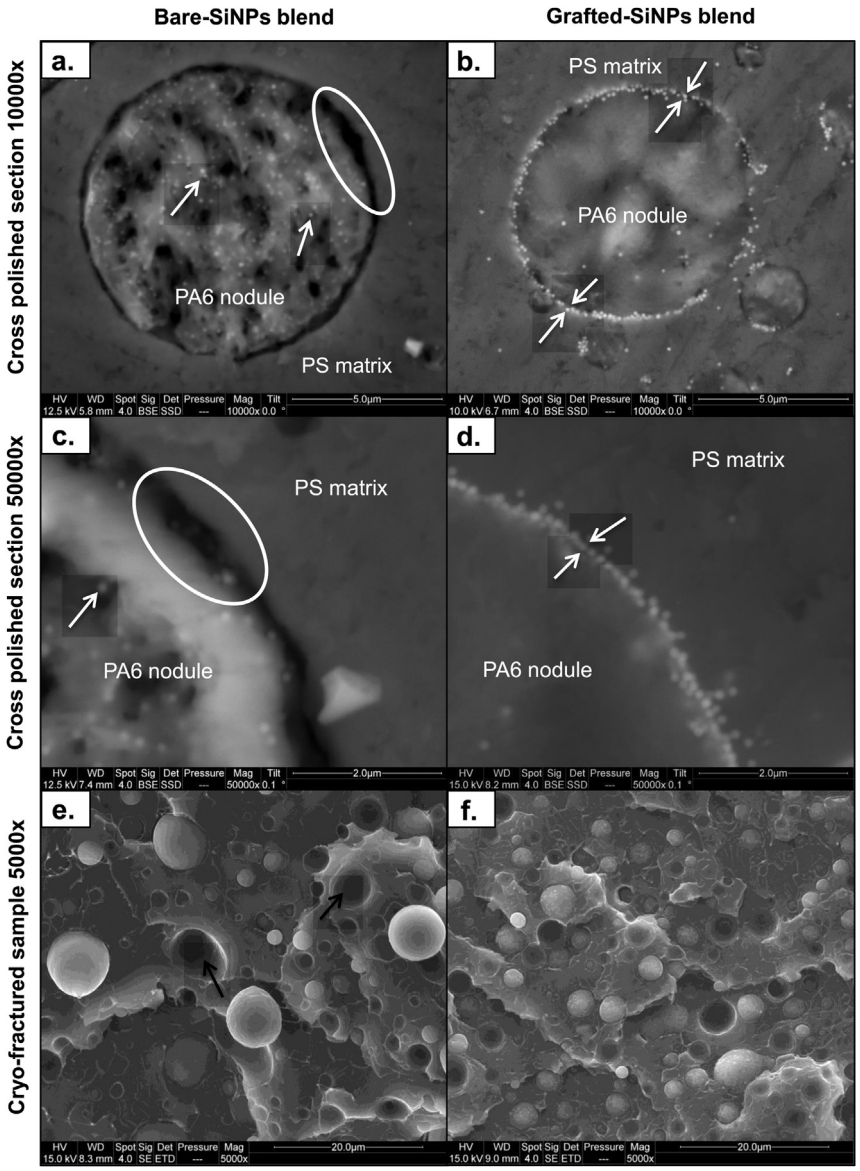

Fig. 7. SEM observations of bare-SiNPs blend (left column) and grafted-SiNPs blend (right column). From upper to lower row: cross polished-section, focus on the PS/PA6 interface and cryo-fractured surface. SiNPs are indicating by white arrows.

grafted-SiNPs at the interface which inhibits coalescence. Micrographs in Fig. 12 illustrate such a solid layer whereas optical microscopic observations of blends in the molten state in the right column of Fig. 11 also confirm the ability of grafted-SiNPs to limit the coalescence process resulting in smaller PA6 nodules.

3.6. Thermal degradation behavior

To investigate the influence of the localization of SiNPs on the thermal degradation behavior of materials, PCFC analyses were carried out. PCFC analyses could be performed according to anaerobic pyrolysis method (method *A*) or under aerobic atmosphere with 20 wt% of oxygen (method *B*). These methods are described in the ASTM D7309. Most generally, anaerobic pyrolysis is applied. Nevertheless, aerobic atmosphere could be used in order to highlight some effects such as resistance to thermo-oxidation or oxygen diffusion barrier. HRR of pure polymers and blends as a function of pyrolysis temperature according to the two discussed methods above are plotted in Fig. 13. TGA under nitrogen and air flow are also performed and used for the determination of the EHC_i and EHC_m parameters according to Equations (2) and (3), respectively. Main thermal degradation values are displayed in Table 2 for anaerobic pyrolysis method and Table 3 for the aerobic one.

HRR curves of pure PS and PA6 with corresponding linear rules of mixture (LRM) (measured according to the methods *A* and *B*) are shown in the upper row of Fig. 13 whereas the PS/PA6 blends are plotted in the lower one. First, no great difference is observed between the blends when the pyrolysis is anaerobic (left column of Fig. 13). Degradation starts around 350 °C and the peak of HRR (pHRR) is observed at 430 ± 5 °C. Despite the fact that PA6 and PS degrade separately (pHRR are 430 and 467 °C for PA6 and PS, respectively), only one peak is noticed for blends due to the overlapping of both steps of decomposition. All flammability characteristics (pHRR, THR, EHC and TML at the end of the degradation – see Table 2) are similar for the three blends and close to the values calculated from a linear rule of mixture.

On the contrary, great differences can be noticed when pyrolysis is aerobic (right column of Fig. 13). The pHRR of the unfilled blend is

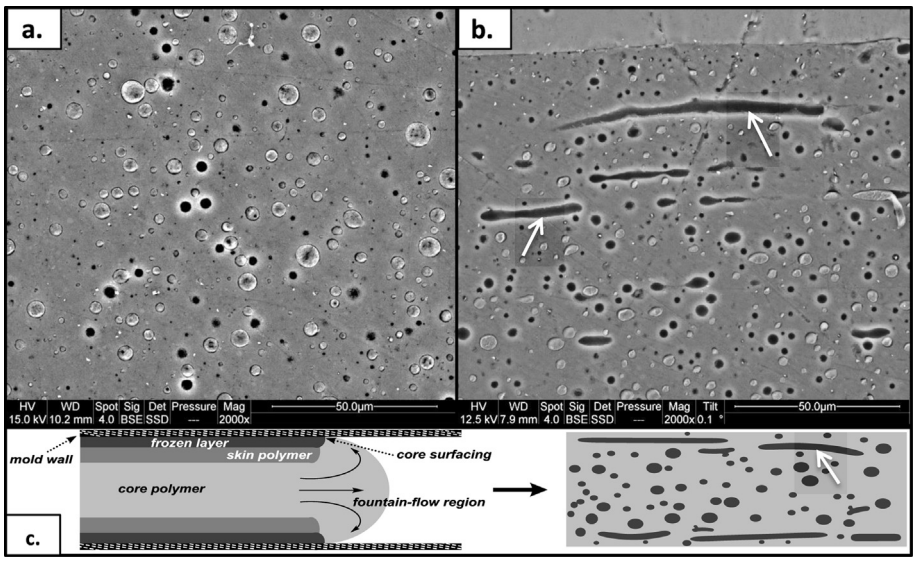

Fig. 8. Cross polished section of neat PS/PA6 blend in perpendicular (a) and parallel (b) directions to extrusion direction. Schematic illustrations of fountain-flow process and its impact on the PA dispersed phases (c).

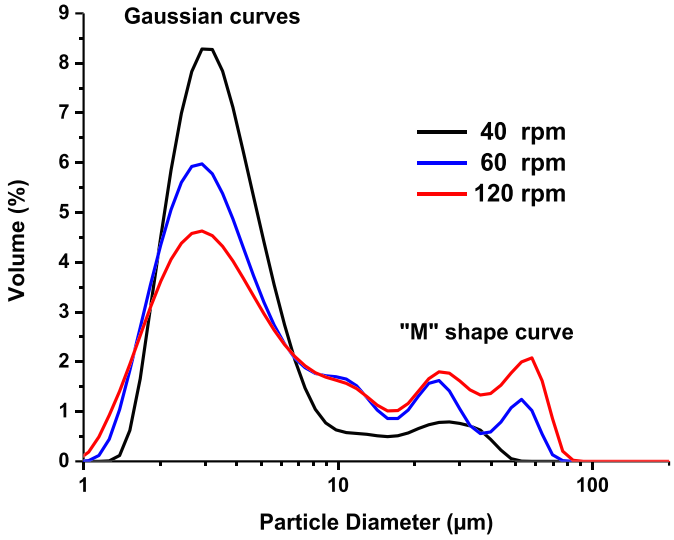

Fig. 9. Size distribution of PA6 dispersed phases of the unfilled PS/PA6 blend as a function of the screw speed of the mini-extruder.

very high (1140 W/g – see Table 3) and much higher than the value calculated from a linear rule of mixture (563 W/g). It means that the decompositions of both polymers are influenced by each other. Interestingly, this phenomenon is observed only when pyrolysis is aerobic, i.e. when oxygen can interfere in the degradation pathway. The bare-SiNPs blend exhibits a similar behavior than the unfilled one, with a slightly lower pHRR (983 W/g). In this case, bare-SiNPs contained in PA6 nodules do not significantly modify the degradation pathway of the polymer blend. But a strong modification of the HRR curve is observed when the grafted-SiNPs are located at the interface between both polymers. In that last case, pHRR is much lower (564 W/g) than for unfilled and bare-SiNPs blends and a small shoulder can be noticed at high temperature (above 450 °C). The grafted-SiNPs blend HRR curve becomes similar to the calculated linear rule of mixing.

According to the above results, grafted-SiNPs can modify the flammability of the blend in a large extent when they are located at the interface and only when pyrolysis is carried out in presence of oxygen. More specifically, the aerobic degradation of both polymers seems to occur independently when grafted-SiNPs are present at

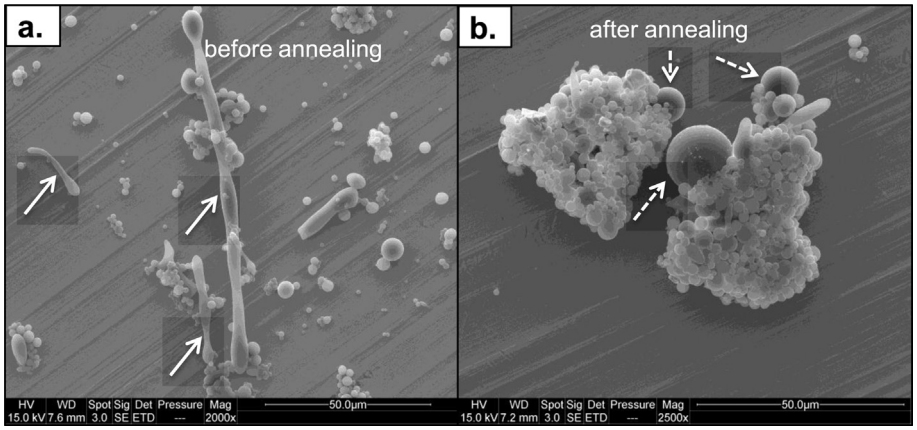

Fig. 10. Micrographs of the PA6 extracted nodules of the unfilled blend before (a) and after (b) annealing. White arrows indicate elongated nodules before (filled) and after (dotted) relaxation process.

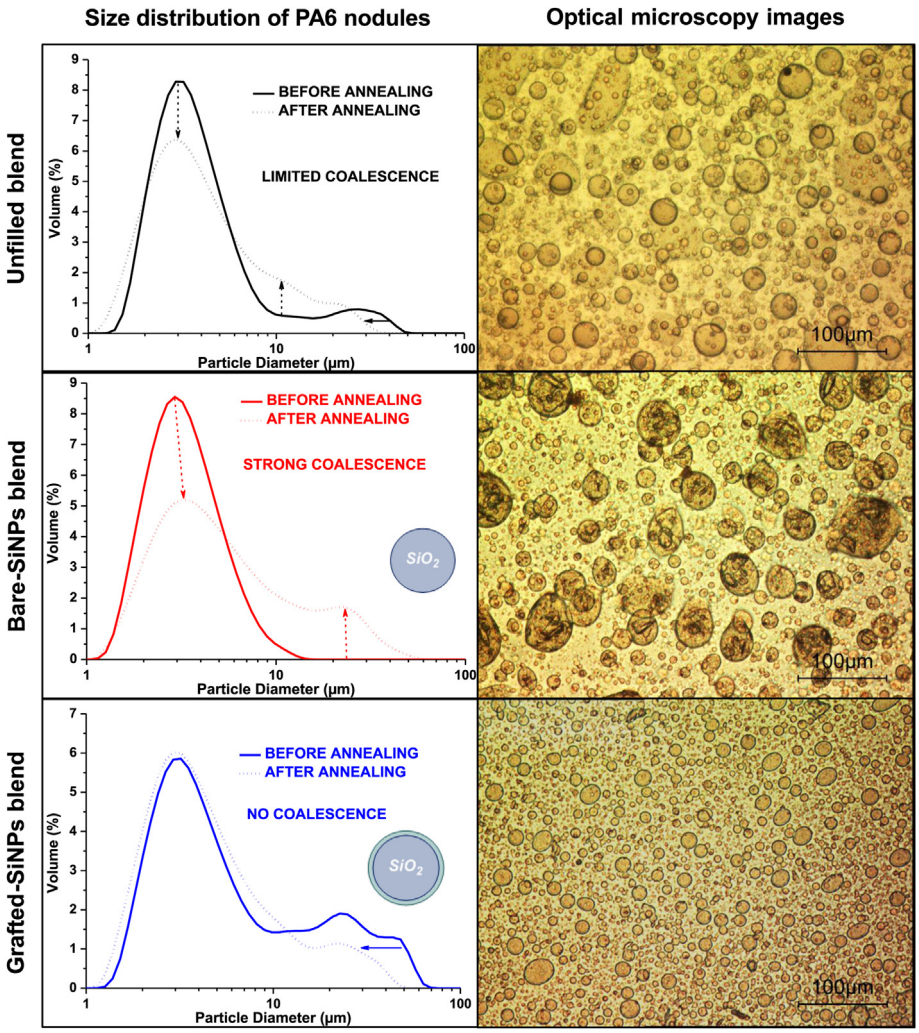

Fig. 11. Left column displays size distribution curves of dispersed PA6 phases before (filled curves) and after (dotted curves) annealing using laser diffraction particle size analyzer for unfilled, bare and grafted-SiNPs blends (from up to down, respectively). Corresponding morphology (after annealing) obtained by optical microscope for each blend is given in the right column.

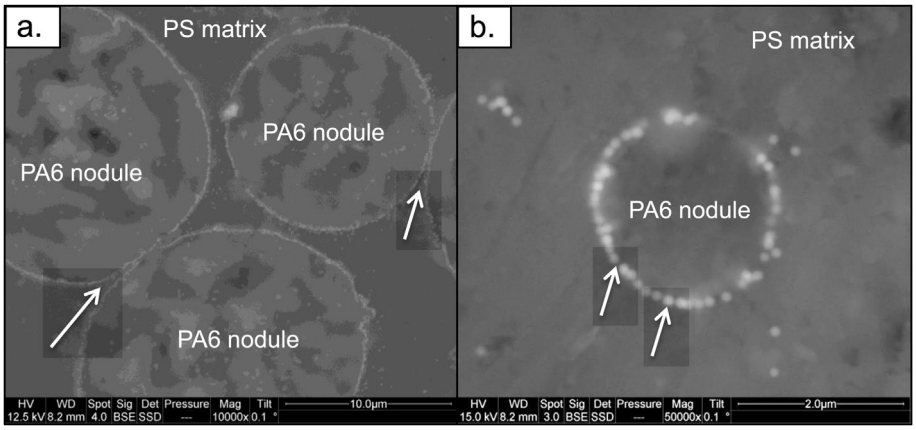

Fig. 12. SEM observations of the solid barrier of grafted-SiNPs at the interface (white arrows) inhibiting coalescence of big (a) and small (b) PA6 nodules.

the interface while strong interactions lead to a very high pHRR in the unfilled blend or when bare-SiNPs are dispersed only in PA6.

Such results can be explained by a modification of gases released at the peak of degradation. Mean EHC_m is approximately similar for the three blends in aerobic and anaerobic conditions because no charring occurs (the entire polymer fraction is degraded). The instantaneous EHC_i changes according to the blend and the pyrolysis. In particular, the value for the grafted-SiNPs blend tested in

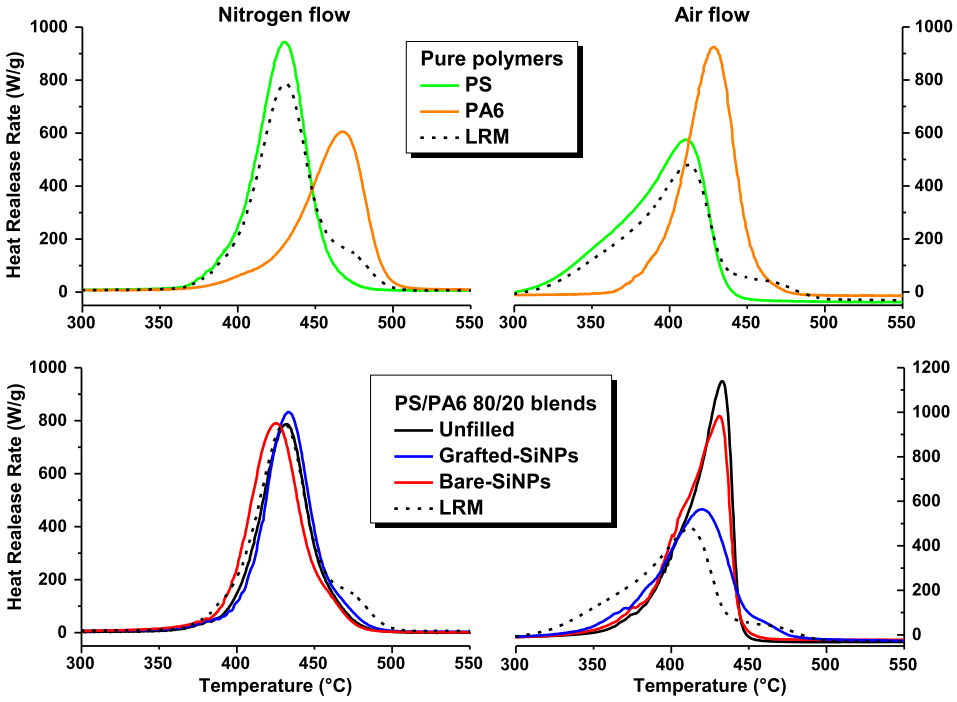

Fig. 13. HRR curves of pure polymers (up) and blends (down) under anaerobic (left) and aerobic (right) pyrolysis. Corresponding linear rules of mixture (LRM) are plotted in each graph (dotted curves).

Table 2
Main thermal degradation values in anaerobic conditions.

Test	Nitrogen atmosphere	pHRR (W/g)	T_{peak} (°C)	THR (kJ/g)	HRC (J/g K)	EHC_m (kJ/g)	EHC_i (kJ/g)	TML at 700 °C (%)
Polymers	PS	937	430	38.8	934	38.9	39.7	99.8
	PA6	597	467	29.2	595	29.4	30.9	99.2
	LRM	869	437	36.9	866	37.0	38.2	99.7
Blends	Unfilled	787	432	32.6	782	32.7	37.6	99.6
	Bare-SiNPs	791	426	33.1	821	34.1	33.5	97.0
	Grafted-SiNPs	833	433	34.4	786	35.3	39.3	97.4

Table 3
Main thermal degradation values in aerobic conditions.

Test	Air atmosphere	pHRR (W/g)	T_{peak} (°C)	THR (kJ/g)	HRC (J/g K)	EHC_m (kJ/g)	EHC_i (kJ/g)	TML at 700 °C (%)
Polymers	PS	604	410	33.0	589	33.1	28.2	99.8
	PA6	398	447	24.1	390	24.2	20.1	99.6
	LRM	563	418	31.2	549	31.3	26.7	99.8
Blends	Unfilled	1140	433	30.4	1156	30.6	48.9	99.5
	Bare-SiNPs	983	431	30.2	989	31.2	38.4	96.8
	Grafted-SiNPs	564	420	31.4	581	32.8	25.3	95.6

aerobic conditions is much lower than that measured for the other blends and close to the corresponding LRM (25.3 kJ/g versus 26.7 kJ/g, see Table 3). The combustion of the pyrolysis gases released at the temperature corresponding to the pHRR generates lower heat. It may be proposed that SiNPs at the interface prevent interactions between degradation products of PS and PA6 phases. Therefore, their degradation seems to occur separately and fit correctly with the corresponding linear rule of mixing. This assumption needs to be assessed by further analyses.

4. Conclusion

The incorporation of modified and unmodified SiNPs into immiscible PS/PA6 80/20 blend was investigated. According to wetting parameter calculations and SEM observations it can be assumed that final localization of bare and grafted SiNPs are in agreement with thermodynamic considerations. Indeed bare-SiNPs totally migrate from PS matrix to dispersed PA6 phases whereas grafted-SiNPs segregate at the interface. These modified SiNPs at the interface not only seem to enhance the cohesion between both polymer phases, but also limit the coalescence process of PA6 nodules, as demonstrated by annealing tests. Hence, these grafted SiNPs at the interface act as a physical barrier layer.

Moreover, this solid barrier of SiNPs at the interface also modifies the aerobic thermal degradation pathway at PCFC tests. In the presence of oxygen, the detrimental effect observed for unfilled and bare-SiNPs blends disappears when the grafted-SiNPs are segregated at the interface.

As a perspective, the nature of the gases released but also the impact of modified SiNPs at the interface on mechanical properties should be scrutinized.

Acknowledgments

The authors acknowledge Nicolas Le Moigne for optical microscopic measurements and Jean-Marie Taulemesse for SEM observations.

Appendix A. Supplementary material

Supplementary data related to this article can be found at http://dx.doi.org/10.1016/j.polymer.2014.04.016.

References

[1] Xanthos M. Interfacial agents for multiphase polymer systems: recent advances. Polym Eng Sci 1988;28:1392–400. http://dx.doi.org/10.1002/pen.760282108.
[2] Duin V, Jerome R, Koning C. Strategies for compatibilization of polymer blends. Prog Polym Sci 1998;23:707–57. http://dx.doi.org/10.1016/S0079-6700(97)00054-3.
[3] Veenstra H, van Lent BJJ, van Dam J, Posthuma de Boer A. Co-continuous morphologies in polymer blends with SEBS block copolymers. Polymer 1999;40:6661–72. http://dx.doi.org/10.1016/S0032-3861(98)00875-1.
[4] Zhang C-L, Feng L-F, Zhao J, Huang H, Hoppe S, Hu G-H. Efficiency of graft copolymers at stabilizing co-continuous polymer blends during quiescent annealing. Polymer 2008;49:3462–9. http://dx.doi.org/10.1016/j.polymer.2008.06.003.
[5] Bhadane PA, Tsou AH, Cheng J, Favis BD. Morphology development and interfacial erosion in reactive polymer blending. Macromolecules 2008;41:7549–59. http://dx.doi.org/10.1021/ma801390s.
[6] Tol R, Groeninckx G, Vinckier I, Moldenaers P, Mewis J. Phase morphology and stability of co-continuous (PPE/PS)/PA6 and PS/PA6 blends: effect of rheology and reactive compatibilization. Polymer 2004;45:2587–601. http://dx.doi.org/10.1016/j.polymer.2003.12.072.
[7] Cigana P, Favis BD, Jerome R. Diblock copolymers as emulsifying agents in polymer blends: influence of molecular weight, architecture, and chemical composition. J Polym Sci B Polym Phys 1996;34:1691–700. http://dx.doi.org/10.1002/(SICI)1099-0488(19960715)34:9<1691::AID-POLB18>3.0.CO;2–2.
[8] Lyu S, Jones TD, Bates FS, Macosko CW. Role of block copolymers on suppression of droplet coalescence. Macromolecules 2002;35:7845–55. http://dx.doi.org/10.1021/ma020754t.
[9] Li J, Favis BD. Strategies to measure and optimize the migration of the interfacial modifier to the interface in immiscible polymer blends. Polymer 2002;43:4935–45. http://dx.doi.org/10.1016/S0032-3861(02)00277-X.
[10] Yuan Z, Favis BD. Influence of the efficacy of interfacial modification on the coarsening of cocontinuous PS/HDPE blends during quiescent annealing. J Polym Sci B Polym Phys 2006;44:711–21. http://dx.doi.org/10.1002/polb.20733.
[11] Adedeji A, Lyu S, Macosko CW. Block copolymers in homopolymer blends: interface vs micelles. Macromolecules 2001;34:8663–8. http://dx.doi.org/10.1021/ma001944b.
[12] Zhao H, Huang B. Compatibilization of blends of polybutadiene and poly(-methyl methacrylate) with poly(butadiene-block-methyl methacrylate). J Polym Sci B Polym Phys 1998;36:85–93. http://dx.doi.org/10.1002/(SICI)1099-0488(19980115)36:1<85::AID-POLB10>3.0.CO;2-A.
[13] Fine T, Pascault J-P. Structured thermoplastic/thermoset blends using block copolymers. Macromol Symp 2006;245–246:375–85. http://dx.doi.org/10.1002/masy.200651352.
[14] Mathew M, Thomas S. Compatibilisation of heterogeneous acrylonitrile–butadiene rubber/polystyrene blends by the addition of styrene–acrylonitrile copolymer: effect on morphology and mechanical properties. Polymer 2003;44:1295–307. http://dx.doi.org/10.1016/S0032-3861(02)00356-7.
[15] Lipatov YS, Nesterov AE. Effect of filler concentration on the phase separation in poly(vinyl acetate)–poly(methyl methacrylate) mixtures. Polym Eng Sci 1992;32:1261–3. http://dx.doi.org/10.1002/pen.760321712.
[16] Fenouillot F, Cassagnau P, Majesté J-C. Uneven distribution of nanoparticles in immiscible fluids: morphology development in polymer blends. Polymer 2009;50:1333–50. http://dx.doi.org/10.1016/j.polymer.2008.12.029.
[17] Pickering SU. CXCVI – emulsions. J Chem Soc Trans 1907;91:2001. http://dx.doi.org/10.1039/ct9079102001.
[18] Sumita M, Sakata K, Asai S, Miyasaka K, Nakagawa H. Dispersion of fillers and the electrical conductivity of polymer blends filled with carbon black. Polym Bull 1991;25:265–71. http://dx.doi.org/10.1007/BF00310802.
[19] Elias L, Fenouillot F, Majesté JC, Alcouffe P, Cassagnau P. Immiscible polymer blends stabilized with nano-silica particles: rheology and effective interfacial tension. Polymer 2008;49:4378–85. http://dx.doi.org/10.1016/j.polymer.2008.07.018.
[20] Martins CG, Larocca NM, Paul DR, Pessan LA. Nanocomposites formed from polypropylene/EVA blends. Polymer 2009;50:1743–54. http://dx.doi.org/10.1016/j.polymer.2009.01.059.
[21] Médéric P, Ville J, Huitric J, Moan M, Aubry T. Effect of processing procedures and conditions on structural, morphological, and rheological properties of polyethylene/polyamide/nanoclay blends. Polym Eng Sci 2011;51:969–78. http://dx.doi.org/10.1002/pen.21825.
[22] Zhang L, Wan C, Zhang Y. Investigation on morphology and mechanical properties of polyamide 6/maleated ethylene-propylene-diene rubber/organoclay composites. Polym Eng Sci 2009;49:209–16. http://dx.doi.org/10.1002/pen.21201.
[23] Gubbels F, Jerome R, Vanlathem E, Deltour R, Blacher SFB. Kinetic and thermodynamic control of the selective localization of carbon black at the interface of immiscible polymer blends. Chem Mater 1998;10:1227–35. http://dx.doi.org/10.1021/cm970594d.
[24] Ali Z, Le HH, Ilisch S, Thurn-Albrecht T, Radusch H-J. Morphology development and compatibilization effect in nanoclay filled rubber blends. Polymer 2010;51:4580–8. http://dx.doi.org/10.1016/j.polymer.2010.08.002.
[25] Liebscher M, Tzounis L, Pötschke P, Heinrich G. Influence of the viscosity ratio in PC/SAN blends filled with MWCNTs on the morphological, electrical, and melt rheological properties. Polymer 2013;54:6801–8. http://dx.doi.org/10.1016/j.polymer.2013.10.040.
[26] Elias L, Fenouillot F, Majesté J-C, Martin G, Cassagnau P. Migration of nano-silica particles in polymer blends. J Polym Sci B Polym Phys 2008;46:1976–83. http://dx.doi.org/10.1002/polb.21534.
[27] Feng J, Chan C, Li J. A method to control the dispersion of carbon black in an immiscible polymer blend. Polym Eng Sci 2003;43:1058–63. http://dx.doi.org/10.1002/pen.10089.
[28] Kaewsaneha C, Tangboriboonrat P, Polpanich D, Eissa M, Elaissari A. Preparation of Janus colloidal particles via pickering emulsion: an overview. Colloids Surf A Physicochem Eng Asp 2013;439:35–42. http://dx.doi.org/10.1016/j.colsurfa.2013.01.004.
[29] Levine S, Bowen BD, Partridge SJ. Stabilization of emulsions by fine particles I. Partitioning of particles between continuous phase and oil/water interface. Colloids Surf 1989;38:325–43. http://dx.doi.org/10.1016/0166-6622(89)80271-9.
[30] Mackay ME, Tuteja A, Duxbury PM, Hawker CJ, Van Horn B, Guan Z, et al. General strategies for nanoparticle dispersion. Science 2006;311:1740–3. http://dx.doi.org/10.1126/science.1122225.
[31] Göldel A, Marmur A, Kasaliwal GR, Pötschke P, Heinrich G. Shape-dependent localization of carbon nanotubes and carbon black in an immiscible polymer blend during melt mixing. Macromolecules 2011;44:6094–102. http://dx.doi.org/10.1021/ma200793a.
[32] Knauert ST, Douglas JF, Starr FW. The effect of nanoparticle shape on polymer-nanocomposite rheology and tensile strength. J Polym Sci B Polym Phys 2007;45:1882–97. http://dx.doi.org/10.1002/polb.21176.
[33] Chung H-J, Kim J, Ohno K, Composto RJ. Controlling the location of nanoparticles in polymer blends by tuning the length and end group of polymer brushes. ACS Macro Lett 2012;1:252–6. http://dx.doi.org/10.1021/mz200068p.
[34] Kwon T, Kim T, Ali FB, Kang DJ, Yoo M, Bang J, et al. Size-controlled polymer-coated nanoparticles as efficient compatibilizers for polymer blends. Macromolecules 2011;44:9852–62. http://dx.doi.org/10.1021/ma2020134.
[35] Walther A, Matussek K, Müller AHE. Engineering nanostructured polymer blends with controlled nanoparticle location using Janus particles. ACS Nano 2008;2:1167–78. http://dx.doi.org/10.1021/nn800108y.
[36] Yang J, Feng C, Dai J, Zhang N, Huang T, Wang Y. Compatibilization of immiscible nylon 6/poly(vinylidene fluoride) blends using graphene oxides. Polym Int 2012;62:1085–93. http://dx.doi.org/10.1002/pi.4396.
[37] Persson AL, Bertilsson H. Viscosity difference as distributing factor in selective absorption of aluminium borate whiskers in immiscible polymer blends. Polymer 1998;39:5633–42. http://dx.doi.org/10.1016/S0032-3861(98)00096-2.
[38] Deyrail Y, Mighri F, Bousmina M, Kaliaguine S. Polyamide/polystyrene blend compatibilisation by montmorillonite nanoclay and its effect on macroporosity of gas diffusion layers for proton exchange membrane fuel cells. Fuel Cells 2007;7:447–52. http://dx.doi.org/10.1002/fuce.200700037.
[39] Fang Z, Harrats C, Moussaif N, Groeninckx G. Location of a nanoclay at the interface in an immiscible poly(ε-caprolactone)/poly(ethylene oxide) blend and its effect on the compatibility of the components. J Appl Polym Sci 2007;106:3125–35. http://dx.doi.org/10.1002/app.26331.
[40] Hong JS, Namkung H, Ahn KH, Lee SJ, Kim C. The role of organically modified layered silicate in the breakup and coalescence of droplets in PBT/PE blends. Polymer 2006;47:3967–75. http://dx.doi.org/10.1016/j.polymer.2006.03.077.
[41] Ray SS, Bousmina M, Maazouz A. Morphology and properties of organoclay modified polycarbonate/poly(methyl methacrylate) blend. Polym Eng Sci 2006;46:1121–9. http://dx.doi.org/10.1002/pen.20598.
[42] Sinha Ray S, Pouliot S, Bousmina M, Utracki LA. Role of organically modified layered silicate as an active interfacial modifier in immiscible polystyrene/polypropylene blends. Polymer 2004;45:8403–13. http://dx.doi.org/10.1016/j.polymer.2004.10.009.
[43] Yousfi M, Soulestin J, Vergnes B, Lacrampe M-F, Krawczak P. Compatibilization of immiscible polymer blends by organoclay: effect of nanofiller or organo-modifier? Macromol Mater Eng 2013;298:757–70. http://dx.doi.org/10.1002/mame.201200138.

[44] Elias L, Fenouillot F, Majeste JC, Cassagnau P. Morphology and rheology of immiscible polymer blends filled with silica nanoparticles. Polymer 2007;48:6029–40. http://dx.doi.org/10.1016/j.polymer.2007.07.061.
[45] Kong M, Huang Y, Chen G, Yang Q, Li G. Retarded relaxation and breakup of deformed PA6 droplets filled with nanosilica in PS matrix during annealing. Polymer 2011;52:5231–6. http://dx.doi.org/10.1016/j.polymer.2011.08.052.
[46] Laoutid F, Estrada E, Michell RM, Bonnaud L, Müller AJ, Dubois P. The influence of nanosilica on the nucleation, crystallization and tensile properties of PP–PC and PP–PA blends. Polymer 2013;54:3982–93. http://dx.doi.org/10.1016/j.polymer.2013.05.031.
[47] Martin G, Barres C, Sonntag P, Garois N, Cassagnau P. Co-continuous morphology and stress relaxation behaviour of unfilled and silica filled PP/EPDM blends. Mater Chem Phys 2009;113:889–98. http://dx.doi.org/10.1016/j.matchemphys.2008.08.069.
[48] Huitric J, Ville J, Médéric P, Moan M, Aubry T. Rheological, morphological and structural properties of PE/PA/nanoclay ternary blends: effect of clay weight fraction. J Rheol 2009;53:1101. http://dx.doi.org/10.1122/1.3153551.
[49] Khatua BB, Lee DJ, Kim HY, Kim JK. Effect of organoclay platelets on morphology of nylon-6 and poly(ethylene-ran-propylene) rubber blends. Macromolecules 2004;37:2454–9. http://dx.doi.org/10.1021/ma0352072.
[50] Zhang C-L, Feng L-F, Gu X-P, Hoppe S, Hu G-H. Efficiency of graft copolymers as compatibilizers for immiscible polymer blends. Polymer 2007;48:5940–9. http://dx.doi.org/10.1016/j.polymer.2007.07.042.
[51] Gao J, Huang C, Wang N, Yu W, Zhou C. Phase separation of poly(methyl methacrylate)/poly(styrene-co-acrylonitrile) blends in the presence of silica nanoparticles. Polymer 2012;53:1772–82. http://dx.doi.org/10.1016/j.polymer.2012.02.027.
[52] Huang Y, Pemberton JE. Synthesis of uniform, spherical sub-100nm silica particles using a conceptual modification of the classic LaMer model. Colloids Surf A Physicochem Eng Asp 2010;360:175–83. http://dx.doi.org/10.1016/j.colsurfa.2010.02.031.
[53] Pegoretti A, Dorigato A, Brugnara M, Penati A. Contact angle measurements as a tool to investigate the filler–matrix interactions in polyurethane–clay nanocomposites from blocked prepolymer. Eur Polym J 2008;44:1662–72. http://dx.doi.org/10.1016/j.eurpolymj.2008.04.011.
[54] Owens DK, Wendt RC. Estimation of the surface free energy of polymers. J Appl Polym Sci 1969;13:1741–7. http://dx.doi.org/10.1002/app.1969.070130815.
[55] Lyon RE, Walters RN. Pyrolysis combustion flow calorimetry. J Anal Appl Pyrolysis 2004;71:27–46. http://dx.doi.org/10.1016/S0165-2370(03)00096-2.
[56] Huggett C. Estimation of rate of heat release by means of oxygen consumption measurements. Fire Mater 1980;4:61–5. http://dx.doi.org/10.1002/fam.810040202.
[57] Lin I-C, Liang M, Liu T-Y, Jia Z, Monteiro MJ, Toth I. Effect of polymer grafting density on silica nanoparticle toxicity. Bioorg Med Chem 2012;20:6862–9. http://dx.doi.org/10.1016/j.bmc.2012.09.045.
[58] Ek S. Determination of the hydroxyl group content in silica by thermogravimetry and a comparison with 1H MAS NMR results. Thermochim Acta 2001;379:201–12. http://dx.doi.org/10.1016/S0040-6031(01)00618-9.
[59] Mueller R, Kammler HK, Wegner K, Pratsinis SE. OH surface density of SiO_2 and TiO_2 by thermogravimetric analysis. Langmuir 2003;19:160–5. http://dx.doi.org/10.1021/la025785w.
[60] Hashemi-Nasab R, Mirabedini SM. Effect of silica nanoparticles surface treatment on in situ polymerization of styrene–butyl acrylate latex. Prog Org Coat 2013;76:1016–23. http://dx.doi.org/10.1016/j.porgcoat.2013.02.016.
[61] Abboud M, Turner M, Duguet E, Fontanille M. PMMA-based composite materials with reactive ceramic fillers. Part 1—chemical modification and characterisation of ceramic particles. J Mater Chem 1997;7:1527. http://dx.doi.org/10.1039/a700573c.
[62] Bourgeat-Lami E. Poly(ethyl acrylate) latexes encapsulating nanoparticles of silica: 1. Functionalization and dispersion of silica. Polymer 1995;36:4385–9. http://dx.doi.org/10.1016/0032-3861(95)96843-W.
[63] Watanabe R, Yokoi T, Kobayashi E, Otsuka Y, Shimojima A, Okubo T, et al. Extension of size of monodisperse silica nanospheres and their well-ordered assembly. J Colloid Interf Sci 2011;360:1–7. http://dx.doi.org/10.1016/j.jcis.2010.09.001.
[64] Cortalezzi MM, Colvin V, Wiesner MR. Controlling submicron-particle template morphology: effect of solvent chemistry. J Colloid Interf Sci 2005;283:366–72. http://dx.doi.org/10.1016/j.jcis.2004.08.171.
[65] Xing P, Bousmina M, Rodrigue D, Kamal MR. Critical experimental comparison between five techniques for the determination of interfacial tension in polymer blends: model system of polystyrene/polyamide-6. Macromolecules 2000;33:8020–34. http://dx.doi.org/10.1021/ma000537x.
[66] Abdelmouleh M, Boufi S, Belgacem MN, Duarte AP, Ben Salah A, Gandini A. Modification of cellulosic fibres with functionalised silanes: development of surface properties. Int J Adhes Adhes 2004;24:43–54. http://dx.doi.org/10.1016/S0143-7496(03)00099-X.
[67] Sundararaj U, Macosko CW. Drop breakup and coalescence in polymer blends: the effects of concentration and compatibilization. Macromolecules 1995;28:2647–57. http://dx.doi.org/10.1021/ma00112a009.